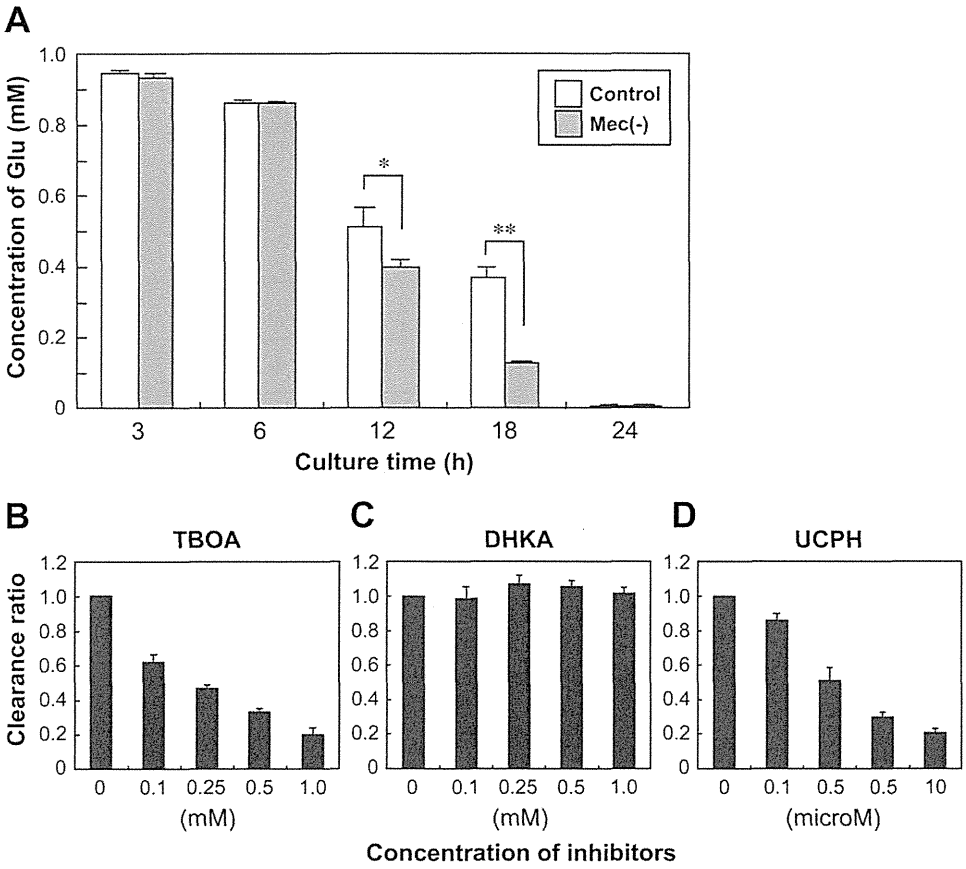

Figure 4. Comparison of glutamate clearance in wild-type and MeCP2-null astrocytes. A. Time-dependent reduction of extracelluar Glu concentration in wild-type (white column) and MeCP2-null (gray column) astrocyte cultures. After treatment with 1.0 mM Glu, culture supernatant was collected at the indicated times for the determination of Glu concentration. The graph shows the concentration of Glu in control and MeCP2-null astrocyte culture medium. Bars represent the means ± SE of samples from three independent experiments (*$p<0.05$). **B–D.** Effects of inhibitors of glutamate transporters (**B,** TBOA; **C,** DHKA; **D,** UCPH) on Glu clearance. Astrocytes were exposed to the indicated concentration of Glu transporter inhibitors, and then 0.1 mM Glu was added; culture supernatant was collected for the determination of Glu concentration at 2 h. The graphs show the clearance ratio upon treatment with each inhibitor. The clearance ratio in the indicated concentration groups was expressed by defining the control level (no inhibitor) as 1.0. Bars represent the means ± SE of samples from three independent experiments.
doi:10.1371/journal.pone.0035354.g004

are responsible for altered translational control in MeCP2 mutant neuron [38]. These findings suggest that a deficit in protein synthesis and/or turnover in the MeCP2-null astrocytes might influence the final levels of GS protein. Further studies are necessary to investigate whether MeCP2 deficiency impairs the synthesis and turnover of proteins in RTT.

The most important finding in this study was that MeCP2 deficiency in astrocytes accelerates Glu clearance. Consistent with this, RTT is associated with abnormalities in the Glu metabolism [24]. Some studies have demonstrated increases in Glu levels in the cerebrospinal fluid (CSF) of human RTT patients [18,19]. On the other hand, in animal studies there have been instances of decreased Glu levels and/or Glu/Gln ratios, as determined by in MR spectroscopy [8,21,22,23]. Furthermore, MeCP2-deficient microglia release an abnormally high level of Glu, causing excitotoxicity that may contribute to dendritic and synaptic abnormalities in RTT [11]. These results clearly suggest that MeCP2 has the potential to regulate Glu levels in the brain under certain circumstances. Glu levels are altered in the RTT brain, but the mechanisms responsible for the changes in Glu metabolism are unknown. In light of our findings, we speculate that abnormal expression of Glu transporters and GS resulting from MeCP2 deficiency could lead to abnormal Glu clearance in astrocytes and in turn to altered levels of Glu in RTT brain. Additional studies are needed to determine the mechanisms underlying changes in Glu levels and Glu metabolism, and their role in the RTT brain.

In conclusion, MeCP2 modulates Glu clearance through the regulation of astroglial genes in astrocytes. This study suggests a novel role for MeCP2 in astrocyte function; these findings may be useful in exploration of a new approach for preventing the neurological dysfunctions associated with RTT.

Materials and Methods

Cell culture

For each experiment, primary cultures were generated from individual MeCP2-null neonates and their wild-type littermates; tail snips from each neonate were obtained for genotyping, as described below. Enriched cultures of GFAP-expressing astroglial cells, which are virtually free of neurons and microglial cells, were established from the cerebral hemispheres of postnatal day (P) 0 to P1 newborn mice, as previously described [29]. In brief, pieces of dissected tissue were trypsinized (0.05%) for 10 min in Ca_2^+- and Mg_2^+-free phosphate-buffered saline (PBS) supplemented with

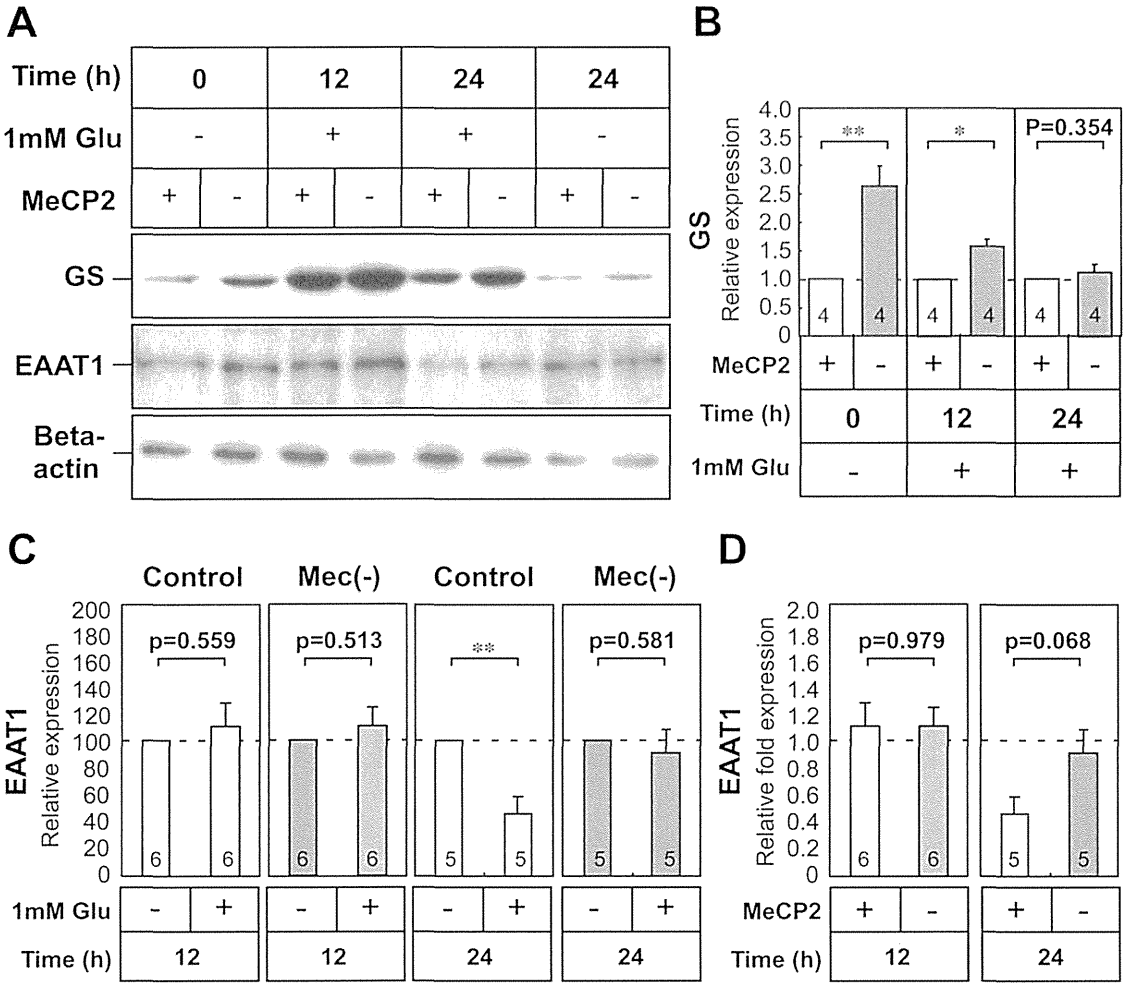

Figure 5. Effect of glutamate on glutamine synthetase and EAAT1 protein expression in MeCP2-null astrocytes. A. Time-dependent expression of GS and EAAT1 proteins in wild-type and MeCP2-deficient astrocyte cultures. Astrocytes were treated with 1.0 mM Glu for 24 h, and subsequently analyzed for expression of GS and EAAT1 by Western blot analysis. Beta-actin protein levels were analyzed in the same way, as an internal control. **B.** The immunoreactive GS protein bands were quantified by densitometry, normalized against β-actin levels, and expressed as fold change relative to the controls (equals 1.0). Bars represent the means ± SE of samples from three independent experiments (*$p<0.05$, **$p<0.01$). Numbers in each column indicate the total number of samples analyzed. **C.** The immunoreactive EAAT1 protein bands were quantified by densitometry, normalized against β-actin levels, and expressed as % of controls (equals 100%). Bars represent the means ± SE of samples from three independent experiments (**$p<0.01$). **D.** Comparison of the effects of Glu on EAAT1 expression in wild-type and MeCP2-null astrocytes. The ratio of EAAT1/β-actin in each treatment group was normalized against that of the non-treated astrocytes from each group. Bars represent the means ± SE of samples from three independent experiments. Numbers in each column indicate the total number of samples analyzed.
doi:10.1371/journal.pone.0035354.g005

0.02% EDTA. Tissue samples were subsequently dissociated in Hank's balanced salt solution (HBSS) containing 15% fetal calf serum (FCS; F2442, Sigma-Aldrich, Inc., St. Louis, MO, USA) by trituration though 10-ml plastic pipettes. Cells were pelleted at 100×g for 5 min, resuspended in Dulbecco's modified Eagle's medium (D-MEM; Wako Pure Chemical Industries, Ltd., Osaka, Japan) containing 15% FCS, and seeded into 100-mm culture dishes previously coated with poly-D-lysine (0.1 mg/ml; Wako Pure Chemical Industries, Ltd., Osaka, Japan). Upon reaching confluency, cells were trypsinized and replated. Cells were used after the third passage (P3) in all experiments, and were seeded at 3×10^4 cells/cm^2 in 6-well plate dishes or 35-mm culture dishes. Cultures were assayed by immunochemical analysis using antibodies against GFAP, MAP2, and CD11b in order to determine the degree of enrichment; the astrocyte cultures were nearly pure without contamination of microglia and neurons (Fig. S3 and Information S1).

Cell growth and bromo-2′-deoxyuridine (BrdU) uptake assay

To determine growth rate, cells were plated at 2×10^5 cells/dish in 35-mm dishes. At each passage, three dishes per cell line were harvested by trypsinization, and cell numbers were determined using a hemocytometer. Growth rate was expressed as the number of harvested cells divided by the number of seeded cells.

BrdU incorporation during DNA synthesis was determined using the 5-Bromo-2′-deoxy-uridine Labeling and Detection Kit I (Roche, Indianapolis, IN, USA). Briefly, cells were seeded at 3.0×10^4 cells per well in 48-well culture plates and incubated in D-MEM containing 10% FCS at 37°C for 24 h. After cells were

Table 1. PCR primers.

	Sense	Antisense	Ta	cycles
GFAP	5′-ATCCGCTCAGGTCATCTTACCC-3′	5′-TGTCTGCTCAATGTCTTCCCTACC-3′	63	25
S100β	5′-AGAGGACTCCAGCAGCAAAGG-3′	5′-AGAGAGCTCAGCTCCTTCGAG-3′	59	32
EAAT1	5′-GAAGTCTCCCAGACGTTCTAATCC-3′	5′-GCTCTGAAACCGCCACTTACTATC-3′	65	35
EAAT2	5′-ATGCTCATCCTCCCTCTTATCATC-3′	5′-CTTTCTTTGTCACTGTCTGAATCTG-3′	63	32
GS	5′-TGTACCTCCATCCTGTTGCC-3′	5′-GTCCCCGTAATCTTGACTCC-3′	57	25
HPRT	5′-CCTGCTGGATTACATTAAAGCACTG-3′	5′-AAGGGCATATCCAACAACAA-3′	57	30
MeCP2	5′-GGTAAAACCCGTCCGGAAAATG-3′	5′-TTCAGTGGCTTGTCTCTGAG-3′	61	35

GFAP, glial fibrillary acidic protein; EAAT, excitatory amino acid transporter; GS, glutamine synthetase; HPRT, hypoxantine-phosphoribosyl-transferase; MeCP2, methyl-CpG-binding protein 2; Ta, annealing temperature (°C).
doi:10.1371/journal.pone.0035354.t001

incubated with 10 μM BrdU for 2 h, they were fixed with 70% ethanol in 50 mM glycine (pH 2.0) for 20 min at −20°C. Cells were incubated with an anti-BrdU monoclonal antibody, followed by a fluorescein-coupled goat anti-mouse Ig and Hoechst33324 (1 μg/ml). To determine the percentages of BrdU-positive cells, fluorescent images were obtained by a Biorevo BZ-9000 fluorescence microscope (KEYENCE Co., Osaka, Japan); images were analyzed using the BZ-II application. BrdU-positive cells and total cells were counted in random 3 fields per well (approximately 1200 cells per well). Results were obtained from four independent experiments.

Cell Viability Analysis

Cell were seeded at 1×10^4 cells per well in 96-well plates and incubated in D-MEM containing 15% FCS at 37°C for 24 h. In injury models of drug and oxidative stress, cells were incubated with 0.01–10 mM glutamate for 24 h, 12.5–200 mM NH_4Cl (Sigma Chemical Co.) for 4 h, or 0.125–1.0 mM H_2O_2 (Wako Pure Chemical Industry, Osaka, Japan) for 1 h as previously described [28,39,40]. After 24 h of drug treatment, cell viability was determined using the WST-8 assay (NACALAI TESQUE, INC., Kyoto, Japan) [39,41].

PCR analysis

MeCP2$^{-/+}$ female mice (B6.129P2(C)-Mecp2$^{tm1.1Bird}$/J strain) were purchased from the Jackson Laboratory (Bar Harbor, ME) and mated with wild-type C57BL/6 male mice. DNA samples were extracted from tail snips from newborn animals; prior to nucleic acid extraction, snips were digested with proteinase K. Genotyping was performed by PCR analysis of genomic DNA according to the protocol provided by the manufacturer (http://jaxmice.jax.org/pub-cgi/protocols/protocols.sh?objtype=protocol&protocol_id=598) [4,12]. All experiments were performed in accordance with the National Institutes of Health Guidelines for the Care and Use of Laboratory Animals, and were approved by the Animal Research Committee of Kurume University.

Total RNA was extracted from cells using a Sepazol RNA I super kit (Nacalai Tesque, Inc., Kyoto, Japan) [41,42]. One microgram of total RNA was reverse transcribed, and 1/100 of the cDNA (equivalent to 10 ng of total RNA) was subjected to PCR amplification with Taq DNA polymerase (Promega, Co., Ltd., Madison, WI) using the following conditions: 25–35 cycles of 94°C for 30 s, annealing temperature for 60 s, and 74°C for 60 s. Primer sets and annealing temperatures are shown in Table 1. The most appropriate PCR conditions for semi-quantitative analysis of each gene were carefully determined by several preliminary experiments (Fig. S4). The number of cycles for GFAP, S100β, EAAT1, EAAT2, and GS was 25, 32, 35, 32, and 25, respectively (Table 1). The amplified cDNA was electrophoresed on 2% agarose gels containing ethidium bromide, and quantities were analyzed by densitometry using ImageJ software (the Research Service Branch of the National Institute of Health, Bethesda, MD, USA) [42]. The relative expression of each gene was normalized to the intensity of a housekeeping gene, hypoxantine-phosphoribosyl-transferase (HPRT; 30 cycles). The expression level of each gene is reported as a ratio relative to the level of normalized expression in a control sample.

Immunocytochemistry

Cultures were fixed with 4% paraformaldehyde for 10 min and permeabilized with 0.05% Triton-X 100 for 5 min. After blocking of nonspecific binding sites with 10% nonfat dry milk in PBS for 1 h, cultures were immunocytochemically stained using antibodies against MeCP2 (anti-MeCP2 polyclonal antibody, MILLIPORE, Temecula, CA, USA; anti-MeCP2 monoclonal antibody, G-6, Santa Cruz Biotechnology, Inc., Santa Cruz, CA), β-tubulin type III (TuJ, Sigma-Aldrich, Inc., St. Louis, Missouri), or glial fibrillary acidic protein (GFAP) (anti-GFAP polyclonal antibody, G9269; anti-GFAP monoclonal antibody, G3893, Sigma-Aldrich, Inc., St. Louis, Missouri), followed by secondary fluorescent antibodies as described previously [12]. Cultures were additionally stained with Hoechst33342 and examined using an Olympus IX-70 (Olympus Japan Inc. Tokyo, Japan) microscope. Photomicrographs were captured using an Olympus DP70 digital camera.

Immunoblotting

Cell extracts were prepared from astroglial cultures as described previously [41]. Western blot analysis was performed using anti-glutamine synthetase (G2781; Sigma-Aldrich, Inc., St. Louis, Missouri), anti-excitatory amino acid transporter 1 (EAAT1, GLAST; Santa Cruz Biotechnology, Inc., Santa Cruz, CA), horseradish peroxidase-conjugated anti-rabbit IgG (DakoCytomation, Glostrup, Denmark), and chemiluminescent substrate (Chemi-Lumi One, NACALAI TESQUE, INC., Kyoto, Japan) [12,41]. Several different exposure times were used for each blot to ensure linearity of band intensities. Immunoreactive bands were quantified using the ImageJ software (Research Service Branch of the National Institute of Health, Bethesda, MD, USA). The relative expression of each protein was normalized to the intensity of β-actin. The expression level of each protein is reported as a

ratio relative to the level of normalized expression in a control sample.

Glutamate Clearance Assay

To measure extracellular glutamate (Glu) concentrations, we used the Glutamate Assay Kit colorimetric assay (Yamasa Corporation, Tokyo, Japan) [43]. Assays were carried out in six independent trials. The clearance ratio of Glu was calculated from the Glu concentration (μM) in the medium sample of the drug-treated astroglial cells (Glu_{drug}) and the control non-drug treated (i.e., treated with drug vehicle alone) glial cells (Glu_{solv}). This is represented mathematically as follows: Glu clearance ratio = $(100-Glu_{drug})/(100-Glu_{solv})$. Threo-beta-benzyloxyaspartate (TBOA), UCPH-101 (2-amino-4-(4-methoxyphenyl)-7-(naphthalen-1-yl)-5-oxo-5,6,7,8-tetrahydro-4H-chromene-3-carbonitrile), or dihydrokainate (DHKA) (all purchased from Tocris Bioscience Ellisville, MO, USA) were applied to astroglial cells 60 min before Glu.

Statistical analysis

Quantitative results are expressed as means ± standard errors (SE). Student's t-test was used to compare data, with $p<0.05$ considered significant.

Supporting Information

Figure S1 BrdU-incorporating cells in wild-type and MeCP2-null astrocytes. The top and bottom pictures show BrdU-incorporating (Green) and Hoechst-stained (Blue) cells, respectively, which were stained with the primary anti-BrdU antibodies, the secondary fluorescein-coupled antibodies, and Hoechst 33324. Negative controls received identical treatments, but were not exposed to BrdU. Representative pictures were used to accurately count the number of BrdU incorporated cells to assess the efficiency of astrocyte cell growth. Scale bar = 200 μm.
(EPS)

Figure S2 Concentration dependency of GS and EAAT1 expression in wild-type and MeCP2-null astrocytes treated with Glutamate. The astrocytes of each group were treated with 0.01–1.0 mM Glu for 12 h, and subsequently analyzed for expression of GS and EAAT1 by western blot analysis.
(EPS)

Figure S3 Purity of astroglial cultures from mouse brain. The purity of astroglial cultures was assessed by immunocytochemisty (**A**) and immunoblotting (**B**) using antibodies against glial fibrillary acidic protein (GFAP; astrocyte marker; Sigma-Aldrich), CD11b (microglial marker; Santacruz), or microtubule associated protein 2 (MAP2; neuronal marker; Sigma-Aldrich). **A.** Immunocytochemistry indicates that neither CD11b nor MAP2 were expressed in astrocyte cultures. Positive control indicates microglia and mouse ES-derived neural cells that stained with anti-CD11b and MAP2 antibodies, respectively. Scale bar = 100 μm. **B.** Western blot analysis of protein extracts from cultured astrocytes and mouse whole brain. Western blot analysis also confirmed that the cultured astrocytes expressed GFAP, but did not express CD11b and MAP2.
(EPS)

Figure S4 Optimization of the semi-quantitative RT-PCR assay. Total RNA extracted from neonatal mouse brain astrocytes was serially diluted (2.5, 5, 10, 20, and 40 ng RNA in lanes 1, 2, 3, 4, and 5, respectively), reverse-transcribed and used as control samples in semi-quantitative RT-PCR for GFAP (**A**), S100β (**B**), HPRT (**C**), EAAT1 (**D**), EAAT2 (**E**), and GS (**F**). PCR was carried out for indicated cycles using each of primer sets shown in Table 1. The amplified cDNA was electrophoresed in a 2% agarose gel containing ethidium bromide. NT, RT-PCR with no template.
(EPS)

Information S1 Supporting materials and methods.
(DOC)

Author Contributions

Conceived and designed the experiments: YO TT. Performed the experiments: YO CM TT. Analyzed the data: YO TT ET. Contributed reagents/materials/analysis tools: KK TM. Wrote the paper: YO TT.

References

1. Chahrour M, Zoghbi HY (2007) The story of Rett syndrome: from clinic to neurobiology. Neuron 56: 422–437.
2. Matsuishi T, Yamashita Y, Takahashi T, Nagamitsu S (2011) Rett syndrome: The state of clinical and basic research, and future perspectives. Brain Dev 33: 623–631.
3. Amir RE, Van den Veyver IB, Wan M, Tran CQ, Francke U, et al. (1999) Rett syndrome is caused by mutations in X-linked MECP2, encoding methyl-CpG-binding protein 2. Nat Genet 23: 185–188.
4. Guy J, Hendrich B, Holmes M, Martin JE, Bird A (2001) A mouse Mecp2-null mutation causes neurological symptoms that mimic Rett syndrome. Nat Genet 27: 322–326.
5. Chen RZ, Akbarian S, Tudor M, Jaenisch R (2001) Deficiency of methyl-CpG binding protein-2 in CNS neurons results in a Rett-like phenotype in mice. Nat Genet 27: 327–331.
6. Calfa G, Percy AK, Pozzo-Miller L (2011) Experimental models of Rett syndrome based on Mecp2 dysfunction. Exp Biol Med (Maywood) 236: 3–19.
7. Bienvenu T, Chelly J (2006) Molecular genetics of Rett syndrome: when DNA methylation goes unrecognized. Nat Rev Genet 7: 415–426.
8. Saywell V, Viola A, Confort-Gouny S, Le Fur Y, Villard L, et al. (2006) Brain magnetic resonance study of Mecp2 deletion effects on anatomy and metabolism. Biochem Biophys Res Commun 340: 776–783.
9. Ballas N, Lioy DT, Grunseich C, Mandel G (2009) Non-cell autonomous influence of MeCP2-deficient glia on neuronal dendritic morphology. Nat Neurosci 12: 311–317.
10. Maezawa I, Swanberg S, Harvey D, LaSalle JM, Jin LW (2009) Rett syndrome astrocytes are abnormal and spread MeCP2 deficiency through gap junctions. J Neurosci 29: 5051–5061.
11. Maezawa I, Jin LW (2010) Rett syndrome microglia damage dendrites and synapses by the elevated release of glutamate. J Neurosci 30: 5346–5356.
12. Okabe Y, Kusaga A, Takahashi T, Mitsumasu C, Murai Y, et al. (2010) Neural development of methyl-CpG-binding protein 2 null embryonic stem cells: a system for studying Rett syndrome. Brain Res 1360: 17–27.
13. Lioy DT, Garg SK, Monaghan CE, Raber J, Foust KD, et al. (2011) A role for glia in the progression of Rett's syndrome. Nature 475: 497–500.
14. Seifert G, Schilling K, Steinhauser C (2006) Astrocyte dysfunction in neurological disorders: a molecular perspective. Nat Rev Neurosci 7: 194–206.
15. Eroglu C, Barres BA (2010) Regulation of synaptic connectivity by glia. Nature 468: 223–231.
16. Sheldon AL, Robinson MB (2007) The role of glutamate transporters in neurodegenerative diseases and potential opportunities for intervention. Neurochem Int 51: 333–355.
17. Eid T, Williamson A, Lee TS, Petroff OA, de Lanerolle NC (2008) Glutamate and astrocytes–key players in human mesial temporal lobe epilepsy? Epilepsia 49 Suppl 2: 42–52.
18. Hamberger A, Gillberg C, Palm A, Hagberg B (1992) Elevated CSF glutamate in Rett syndrome. Neuropediatrics 23: 212–213.
19. Lappalainen R, Riikonen RS (1996) High levels of cerebrospinal fluid glutamate in Rett syndrome. Pediatr Neurol 15: 213–216.
20. Pan JW, Lane JB, Hetherington H, Percy AK (1999) Rett syndrome: 1H spectroscopic imaging at 4.1 Tesla. J Child Neurol 14: 524–528.
21. Horska A, Farage L, Bibat G, Nagae LM, Kaufmann WE, et al. (2009) Brain metabolism in Rett syndrome: age, clinical, and genotype correlations. Ann Neurol 65: 90–97.
22. Ward BC, Kolodny NH, Nag N, Berger-Sweeney JE (2009) Neurochemical changes in a mouse model of Rett syndrome: changes over time and in response to perinatal choline nutritional supplementation. J Neurochem 108: 361–371.

23. Viola A, Saywell V, Villard L, Cozzone PJ, Lutz NW (2007) Metabolic fingerprints of altered brain growth, osmoregulation and neurotransmission in a Rett syndrome model. PLoS One 2: e157.
24. Dunn HG, MacLeod PM (2001) Rett syndrome: review of biological abnormalities. Can J Neurol Sci 28: 16–29.
25. Naidu S, Kaufmann WE, Abrams MT, Pearlson GD, Lanham DC, et al. (2001) Neuroimaging studies in Rett syndrome. Brain Dev 23 Suppl 1: S62–71.
26. Colantuoni C, Jeon OH, Hyder K, Chenchik A, Khimani AH, et al. (2001) Gene expression profiling in postmortem Rett Syndrome brain: differential gene expression and patient classification. Neurobiol Dis 8: 847–865.
27. Setoguchi H, Namihira M, Kohyama J, Asano H, Sanosaka T, et al. (2006) Methyl-CpG binding proteins are involved in restricting differentiation plasticity in neurons. J Neurosci Res 84: 969–979.
28. Chen CJ, Liao SL, Kuo JS (2000) Gliotoxic action of glutamate on cultured astrocytes. J Neurochem 75: 1557–1565.
29. Lehmann C, Bette S, Engele J (2009) High extracellular glutamate modulates expression of glutamate transporters and glutamine synthetase in cultured astrocytes. Brain Res 1297: 1–8.
30. Shigeri Y, Seal RP, Shimamoto K (2004) Molecular pharmacology of glutamate transporters, EAATs and VGLUTs. Brain Res Brain Res Rev 45: 250–265.
31. Erichsen MN, Huynh TH, Abrahamsen B, Bastlund JF, Bundgaard C, et al. (2010) Structure-activity relationship study of first selective inhibitor of excitatory amino acid transporter subtype 1: 2-Amino-4-(4-methoxyphenyl)-7-(naphthalen-1-yl)-5-oxo-5,6,7,8-tetrahydro-4 H-chromene-3-carbonitrile (UCPH-101). J Med Chem 53: 7180–7191.
32. Deguchi K, Antalffy BA, Twohill LJ, Chakraborty S, Glaze DG, et al. (2000) Substance P immunoreactivity in Rett syndrome. Pediatr Neurol 22: 259–266.
33. Namihira M, Nakashima K, Taga T (2004) Developmental stage dependent regulation of DNA methylation and chromatin modification in a immature astrocyte specific gene promoter. FEBS Lett 572: 184–188.
34. Tsujimura K, Abematsu M, Kohyama J, Namihira M, Nakashima K (2009) Neuronal differentiation of neural precursor cells is promoted by the methyl-CpG-binding protein MeCP2. Exp Neurol 219: 104–111.
35. Jellinger K, Armstrong D, Zoghbi HY, Percy AK (1988) Neuropathology of Rett syndrome. Acta Neuropathol 76: 142–158.
36. Kim SY, Choi SY, Chao W, Volsky DJ (2003) Transcriptional regulation of human excitatory amino acid transporter 1 (EAAT1): cloning of the EAAT1 promoter and characterization of its basal and inducible activity in human astrocytes. J Neurochem 87: 1485–1498.
37. Yang Y, Gozen O, Vidensky S, Robinson MB, Rothstein JD (2010) Epigenetic regulation of neuron-dependent induction of astroglial synaptic protein GLT1. Glia 58: 277–286.
38. Ricciardi S, Boggio EM, Grosso S, Lonetti G, Forlani G, et al. (2011) Reduced AKT/mTOR signaling and protein synthesis dysregulation in a Rett syndrome animal model. Hum Mol Genet 20: 1182–1196.
39. Ushikoshi H, Takahashi T, Chen X, Khai NC, Esaki M, et al. (2005) Local overexpression of HB-EGF exacerbates remodeling following myocardial infarction by activating noncardiomyocytes. Lab Invest 85: 862–873.
40. Norenberg MD, Jayakumar AR, Rama Rao KV, Panickar KS (2007) New concepts in the mechanism of ammonia-induced astrocyte swelling. Metab Brain Dis 22: 219–234.
41. Takahashi T, Kawai T, Ushikoshi H, Nagano S, Oshika H, et al. (2006) Identification and isolation of embryonic stem cell-derived target cells by adenoviral conditional targeting. Mol Ther 14: 673–683.
42. Kawai T, Takahashi T, Esaki M, Ushikoshi H, Nagano S, et al. (2004) Efficient cardiomyogenic differentiation of embryonic stem cell by fibroblast growth factor 2 and bone morphogenetic protein 2. Circ J 68: 691–702.
43. Takeuchi H, Mizuno T, Zhang G, Wang J, Kawanokuchi J, et al. (2005) Neuritic beading induced by activated microglia is an early feature of neuronal dysfunction toward neuronal death by inhibition of mitochondrial respiration and axonal transport. J Biol Chem 280: 10444–10454.

CLINICAL GENETICS An International Journal of Genetics, Molecular and Personalized Medicine

Clin Genet 2012: 82: 569–573
Printed in Singapore. All rights reserved

Published by Blackwell Publishing Ltd
CLINICAL GENETICS
doi: 10.1111/j.1399-0004.2011.01819.x

Short Report

FOXG1 mutations in Japanese patients with the congenital variant of Rett syndrome

S Takahashi[a], N Matsumoto[a], A Okayama[a], N Suzuki[a], A Araki[a], K Okajima[a], H Tanaka[b] and A Miyamoto[b]

[a]Department of Pediatrics, Asahikawa Medical University, Asahikawa, Japan and [b]Department of Pediatrics, Asahikawa Habilitation Center for Disabled Children, Asahikawa, Japan

Takahashi S, Matsumoto N, Okayama A, Suzuki N, Araki A, Okajima K, Tanaka H, Miyamoto A. *FOXG1* mutations in Japanese patients with the congenital variant of Rett syndrome.
Clin Genet 2012: 82: 569–573. © John Wiley & Sons A/S. Published by Blackwell Publishing Ltd, 2011

Rett syndrome (RTT) is a severe neurodevelopmental disorder characterized by microcephaly, psychomotor regression, seizures and stereotypical hand movements. Recently, deletions and inactivating mutations in *FOXG1*, encoding a brain-specific transcription factor that is critical for forebrain development, have been found to be associated with the congenital variant of RTT. Here we report the clinical features and molecular characteristics of two cases of the congenital variant of RTT. We conducted mutation screenings of *FOXG1* in a cohort of 15 Japanese patients with a clinical diagnosis of atypical RTT but without *MECP2* and *CDKL5* mutations. Two unrelated female patients had heterozygous mutations (c.256dupC, p.Gln86ProfsX35 and c.689G>A, pArg230His). Both showed neurological symptoms from the neonatal period, including hypotonia, irritability and severe microcephaly. Further, their psychomotor development was severely impaired, as indicated by their inability to sit unaided or acquire speech sounds, and they had a hyperkinetic movement disorder, because both displayed hand stereotypies and jerky movements of the upper limbs. Brain magnetic resonance imaging scans revealed delayed myelination with hypoplasia of the corpus callosum and frontal lobe. These cases confirm the involvement of FOXG1 in the molecular etiology of the congenital variant of RTT and show the characteristic features of FOXG1-related disorder.

Conflict of interest

The authors declare no conflicts of interest.

Key words: congenital variant – *FOXG1* – microcephaly – mutation – Rett syndrome

Corresponding author: Satoru Takahashi, MD, PhD, Department of Pediatrics, Asahikawa Medical University, 2-1-1-1 Midorigaoka-Higashi, Asahikawa, Hokkaido 078–8510, Japan.
Tel.: +81 166 68 2483;
fax: +81 166 68 2489;
e-mail: satoru5p@asahikawa-med.ac.jp

Received 6 September 2011, revised and accepted for publication 28 November 2011

Rett syndrome (RTT) is a neurodevelopmental disorder that is associated with mutations in *MECP2*, encoding methyl-CpG-binding protein 2 (1). Patients with RTT show characteristic clinical features including hypotonia, developmental delay, loss of purposeful hand movements, hand stereotypies and decelerated head growth (2). The clinical severity of RTT varies widely, ranging from the severe 'congenital variant' to the milder 'forme fruste' (3). The congenital variant is characterized by hypotonia and developmental delay beginning earlier than in the typical RTT. *MECP2* mutations are present in 70–90% of the typical RTT cases, but the mutation rate is low in atypical RTT cases (4), suggesting that other genes are responsible for the atypical forms.

Small *de novo* interstitial deletions in 14q12 and a balanced *de novo* translocation [t(2;14)(p22;q12)] with an adjacent small inversion in 14q12 have been identified in cases with clinical features reminiscent of the congenital variant of RTT (5–8). The common deleted region contains *FOXG1*, a gene that encodes a brain-specific transcriptional repressor FOXG1, which promotes progenitor proliferation and suppresses premature neurogenesis for proper forebrain development (9, 10). Both *FOXG1* homozygous- and heterozygous-mutant mice exhibit complex forebrain malformations (9–12). The importance of *FOXG1* was reinforced by the identification of *FOXG1*-null mutations in two unrelated girls with the congenital variant (13). These studies suggest that the congenital

variant of RTT can be caused by point mutations as well as complete deletions in *FOXG1*.

At present, 17 point mutations in *FOXG1* have been reported in patients with the congenital variant of RTT (13–20). Here, we report two *FOXG1* mutations associated with the congenital variant, which confirms the involvement of FOXG1 in the pathophysiology of the congenital variant of RTT and helps to delineate the clinical features associated with *FOXG1* mutations.

Materials and methods

Patients

Fifteen Japanese patients (13 females and 2 males) with a clinical diagnosis of atypical RTT based on the revised criteria for this disorder (2) were examined. Eight and seven patients were considered to have the congenital and early seizure variants, respectively. Direct sequencing of the entire coding sequences and exon–intron boundaries did not reveal *MECP2* and *CDKL5* mutations in these patients. The possibility of large rearrangements in these genes was excluded by using multiplex ligation-dependent probe amplification (MLPA) method (MRC-Holland, Amsterdam, The Netherlands).

Molecular analysis

Blood samples were collected from the patients and their parents after their written informed consent. Genomic DNA was extracted from peripheral blood leukocytes and used as the template for polymerase chain reaction (PCR). Appropriate primers were used to yield DNA fragments spanning the entire *FOXG1* coding region (13). Mutation screenings were performed by direct sequencing of exon1-derived PCR products. Large rearrangements of *FOXG1* DNA were detected by using the MLPA method according to the manufacturer's instructions (MRC-Holland).

Results

Case report

Patient 1

This female patient, now aged 34 years, is the third child of healthy and non-consanguineous parents. She has two healthy brothers. She was born at term by spontaneous delivery after an uneventful pregnancy. Her birth weight was 2570 g and she had a small occipito-frontal circumference (OFC) of 30 cm (third percentile). During the neonatal period, she showed sleep disturbance and inconsolable crying. She was referred to a clinical unit at 7 months of age because of psychomotor retardation. Physical examination revealed severe hypotonia, poor eye contact, strabismus and head growth deceleration. At the age of 1 year, she displayed hand stereotypies with hand-to-mouth movements, tongue protrusion and intermittent bruxism. She also had generalized tonic seizures at that age. Interictal electroencephalogram (EEG) showed focal spike discharges over the left parietal area. The seizures were eventually controlled with sodium valproate and clobazam. Because of feeding problems resulting from swallowing difficulties, she was fed predominantly via a gastrostomy tube. She was never able to sit unaided and never acquired speech sounds or purposeful hand skills. At present, she is permanently bedridden and has severe scoliosis, jerky movements of the upper limbs, self-abusive behavior such as biting her hands and microcephaly (OFC of 46 cm). Brain magnetic resonance imaging (MRI) scans performed at the age of 33 years showed microcephaly with hypoplasia of the frontal lobes and corpus callosum (Fig. 1a,b).

Patient 2

This 8-year-old female patient is the second child of healthy and non-consanguineous parents. She has a healthy brother. She was born at term by spontaneous delivery after an uneventful pregnancy. Her birth weight was 2686 g and she had a relatively small head circumference (OFC of 31 cm; 10th percentile). During the neonatal period, she had strabismus, poor eye contact and inconsolable crying. She was referred to a clinical unit at 2 months of age. Physical examination revealed severe hypotonia and decelerated head growth. Microcephaly became more evident with time (OFCs of 38, 41, 43 and 44 cm at 6 months, 2, 5 and 7 years, respectively, all below the third percentile). The developmental milestones were severely delayed: she acquired head control at 7 months and turned over at 20 months. She displayed prominent hyperkinetic movement disorders with hand stereotypies, jerky movements of the upper limbs and frequent and inappropriate episodes of laughter. At 3 years of age, she had two episodes of hyperthermia-induced seizures. Although interictal EEG revealed focal spike discharges over the right parietal area, the seizures did not recur even without antiepileptic drug treatment. She remains incapable of sitting up unaided, as well as acquiring speech sounds and purposeful hand skills. Brain MRI scans performed at the age of 8 years showed delayed myelination in the frontal lobe with hypoplasia of the corpus callosum and frontal lobe (Fig. 1c,d).

Identification of *FOXG1* mutations

We identified heterozygous *FOXG1* mutations in both patients (Fig. 2). Patient 1 showed duplication of cytosine at nucleotides 256 (c.256dupC, p.Gln86ProfsX35), resulting in the loss of the three main functional domains of FOXG1 (Fig. 2a). This frameshift mutation has also been identified in an unrelated patient (20). Patient 2 showed a novel missense mutation (c.689G>A, p.Arg230His) within the DNA-binding forkhead domain, which affects a residue highly conserved in different species (Fig. 2b). Testing of their parents confirmed that both the mutations were *de novo*. We did not find deletions in *FOXG1* in our cohort.

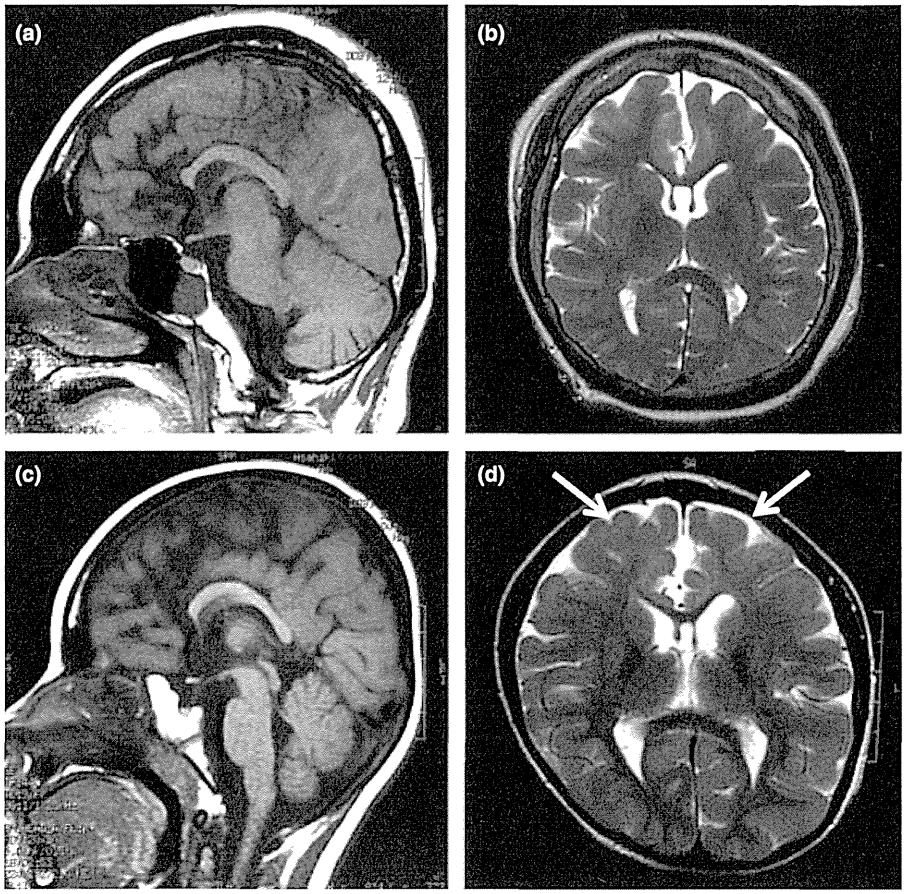

Fig. 1. Brain magnetic resonance imaging (MRI) scans of the two patients with *FOXG1* mutations. Patient 1 (aged 33 years during MRI) has hypoplasia of the frontal lobe and corpus callosum (**a** and **b**). Patient 2 (aged 8 years during MRI) has delayed myelination in the frontal lobe (arrows) with hypoplasia of the corpus callosum and frontal lobe (**c** and **d**). Both have a low forehead which indicates a hypoplastic frontal lobe. (**a**) and (**c**) T1-weighted sagittal images; (**b**) and (**d**) T2-weighted axial images.

Discussion

We identified two heterozygous *FOXG1* mutations in two patients with the congenital variant of RTT. These new cases provide additional support for delineating the clinical features of the FOXG1-related phenotypes. Both the patients had hypotonia and irritability in the neonatal period. Deceleration of head growth, leading to severe microcephaly, was recognized soon afterwards. They also had strabismus and poor eye contact. Their motor development was severely impaired and voluntary hand use was absent. They were unable to sit unaided and did not acquire speech sounds. They showed a prominent hyperkinetic movement disorder, with hand stereotypies and jerky movements of the upper limbs. These clinical features are similar to those previously described in patients with the congenital variant of RTT (13–20).

Large-scale molecular screenings of *FOXG1* have been conducted mainly in female individuals with typical and atypical RTT (14–16). The preponderance of female patients with *FOXG1* mutations may be because of this bias. Recent studies have shown point mutations and deletions in 14q12 in male individuals with the congenital variant of RTT as well (17, 20). Given that *FOXG1* is an autosomal gene, *FOXG1* mutations may be responsible for the clinical features in female and male individuals with this form of RTT. The c.256dupC mutation has been identified in a male patient who presented similar clinical features to those observed in our female patient (20). This recurrent mutation caused duplication of cytosine after seven subsequent cytosines in *FOXG1*, suggesting that this cytosine stretch may be prone to replication errors and present a mutation hotspot in *FOXG1*.

FOXG1 is a DNA-binding transcription factor with a forkhead domain that represses target genes. It recruits transcriptional co-repressor proteins via two protein-binding domains (JARID1B and Groucho-binding domains). Interaction between FOXG1 and its co-repressor proteins is critical for early brain development (21). Missense mutations in the functional domains of FOXG1 or late truncating mutations possibly cause a milder phenotype, because the resulting proteins may retain some functions (16). However, Patient 2, who had a missense mutation of the DNA-binding forkhead domain, presented with a severe phenotype similar to that of Patient 1, who harbored a frameshift mutation that resulted in the loss of the three main

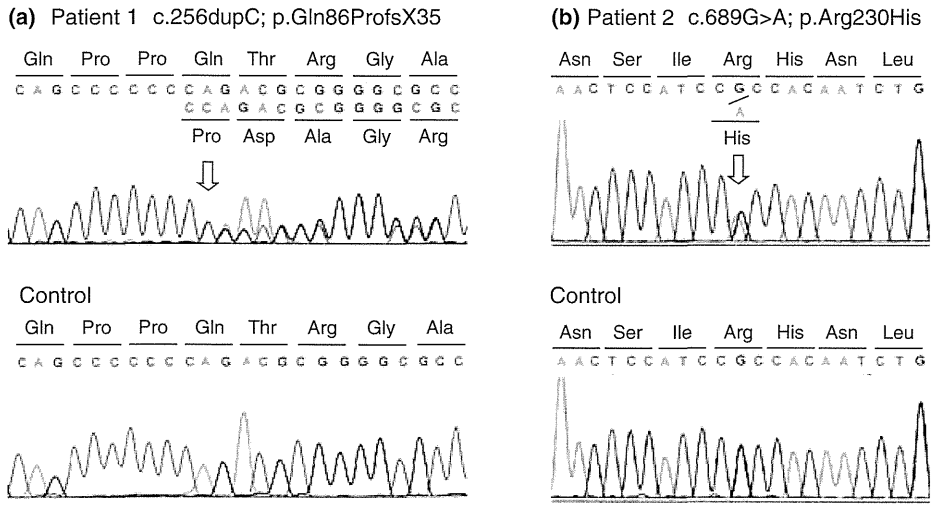

Fig. 2. The *FOXG1* mutations in Patients 1 and 2. Automated DNA sequencing with the polymerase chain reaction product from Patient 1 showed duplication of cytosine at nucleotides 256 (c.256dupC, numbering according to GenBank accession no. NM_005249.3) in *FOXG1* (arrow), which resulted in a shift of the reading frame and introduction of a premature stop codon (p.Gln86ProfsX35) (**a**). In Patient 2, we found a guanine-to-adenine transition at nucleotide 689 (c.689G>A), which resulted in an arginine-to-histidine substitution at amino acid position 230 (p.Arg230His; arrow) (**b**).

functional domains of FOXG1. The missense mutation (p.Arg230His) appeared to affect the affinity of FOXG1 for DNA. Our findings support the idea that a missense mutation in the forkhead domain impairs its target recognition and causes mislocalization of the protein in the nucleus (19). Thus, missense mutations within the DNA-binding domain, as well as clear loss-of-function mutations, can have a severe impact on FOXG1 function. Our data, taken together with previous findings, indicate that the genotype does not predict the severity of the phenotype. Indeed, a late truncating mutation (p.Tyr416X) that affects the C-terminal part of FOXG1 but maintains the three known functional domains reportedly causes the most severe phenotype (14).

FOXG1 plays an important role in forebrain development (10). Brain MRI scans of our two patients showed poor development of the frontal lobe and hypoplasia of the corpus callosum, which are similar to the findings of previous *FOXG1* mutation reports (14, 15, 20). *FOXG1* mutant mice are an interesting animal model for investigating how *FOXG1* haploinsufficiency affects brain development and neuronal function. Although *FOXG1* homozygous-mutant mice die shortly after birth with severe brain defects (9), the heterozygous mutants have less severe brain defects but still exhibit a reduction in the volume of the neocortex, hippocampus and striatum and a thin cortex because of reduced thickness of the superficial cortical layers (12). Furthermore, *FOXG1* heterozygous-mutant mice exhibit learning deficits in fear-condition behavioral tests (11). These animal data are consistent with the findings that humans with *FOXG1* haploinsufficiency have poor forebrain development as well as cognitive and motor defects.

In conclusion, we identified a novel mutation and a recurrent mutation in *FOXG1* in two patients with the congenital variant of RTT. Our data support the involvement of FOXG1 in the molecular etiology of this form of RTT. We suggest that *FOXG1* mutation analysis should be performed in female and male patients with developmental features suggestive of the congenital variant and brain malformations including poor frontal lobe development and hypoplasia of the corpus callosum.

Acknowledgements

We thank the families described here, whose help and participation made this work possible. This work was supported in part by Grant-in-Aid for Scientific Research C from the Japan Society for the Promotion of Science (#22591118).

References

1. Amir RE, Van den Veyver IB, Wan M, Tran CQ, Francke U, Zoghbi HY. Rett syndrome is caused by mutations in X-linked MECP2, encoding methyl-CpG-binding protein 2. Nat Genet 1999: 23: 185–188.
2. Neul JL, Kaufmann WE, Glaze DG et al. Rett syndrome: revised diagnostic criteria and nomenclature. Ann Neurol 2010: 68: 944–950.
3. Hagberg BA, Skjeldal OH. Rett variants: a suggested model for inclusion criteria. Pediatr Neurol 1994: 11: 5–11.
4. Webb T, Latif F. Rett syndrome and the MECP2 gene. J Med Genet 2001: 38: 217–223.
5. Shoichet SA, Kunde SA, Viertel P et al. Haploinsufficiency of novel FOXG1B variants in a patient with severe mental retardation, brain malformations and microcephaly. Hum Genet 2005: 117: 536–544.
6. Bisgaard AM, Kirchhoff M, Tumer Z et al. Additional chromosomal abnormalities in patients with a previously detected abnormal karyotype, mental retardation, and dysmorphic features. Am J Med Genet A 2006: 140: 2180–2187.
7. Jacob FD, Ramaswamy V, Andersen J, Bolduc FV. Atypical Rett syndrome with selective FOXG1 deletion detected by comparative genomic hybridization: case report and review of literature. Eur J Hum Genet 2009: 17: 1577–1581.
8. Mencarelli MA, Kleefstra T, Katzaki E et al. 14q12 Microdeletion syndrome and congenital variant of Rett syndrome. Eur J Med Genet 2009: 52: 148–152.

9. Xuan S, Baptista CA, Balas G, Tao W, Soares VC, Lai E. Winged helix transcription factor BF-1 is essential for the development of the cerebral hemispheres. Neuron 1995: 14: 1141–1152.
10. Hanashima C, Li SC, Shen L, Lai E, Fishell G. Foxg1 suppresses early cortical cell fate. Science 2004: 303: 56–59.
11. Shen Q, Wang Y, Dimos JT et al. The timing of cortical neurogenesis is encoded within lineages of individual progenitor cells. Nat Neurosci 2006: 9: 743–751.
12. Eagleson KL, Schlueter Mc, Fadyen-Ketchum LJ, Ahrens ET et al. Disruption of Foxg1 expression by knock-in of cre recombinase: effects on the development of the mouse telencephalon. Neuroscience 2007: 148: 385–399.
13. Ariani F, Hayek G, Rondinella D et al. FOXG1 is responsible for the congenital variant of Rett syndrome. Am J Hum Genet 2008: 83: 89–93.
14. Bahi-Buisson N, Nectoux J, Girard B et al. Revisiting the phenotype associated with FOXG1 mutations: two novel cases of congenital Rett variant. Neurogenetics 2010: 11: 241–249.
15. Mencarelli MA, Spanhol-Rosseto A, Artuso R et al. Novel FOXG1 mutations associated with the congenital variant of Rett syndrome. J Med Genet. 2010: 47: 49–53.
16. Philippe C, Amsallem D, Francannet C et al. Phenotypic variability in Rett syndrome associated with FOXG1 mutations in females. J Med Genet 2010: 47: 59–65.
17. Kortüm F, Das S, Flindt M et al. The core FOXG1 syndrome phenotype consists of postnatal microcephaly, severe mental retardation, absent language, dyskinesia, and corpus callosum hypogenesis. J Med Genet 2011: 48: 396–406.
18. Roche-Martinez A, Gerotina E, Armstrong-Moron J, Sans-Capdevila O, Pineda M. FOXG1, a new gene responsible for the congenital form of Rett syndrome. Rev Neurol 2011: 52: 597–602.
19. Le Guen T, Fichou Y, Nectoux J et al. A missense mutation within the fork-head domain of the forkhead box G1 gene (FOXG1) affects its nuclear localization. Hum Mutat 2011: 32: E2026–E2035.
20. Le Guen T, Bahi-Buisson N, Nectoux J et al. A FOXG1 mutation in a boy with congenital variant of Rett syndrome. Neurogenetics 2011: 12: 1–8.
21. Yao J, Lai E, Stifani S. The winged-helix protein brain factor 1 interacts with groucho and hes proteins to repress transcription. Mol Cell Biol 2001: 21: 1962–1972.

Journal of Human Genetics (2014) 59, 292–295

www.nature.com/jhg

SHORT COMMUNICATION

De novo WDR45 mutation in a patient showing clinically Rett syndrome with childhood iron deposition in brain

Chihiro Ohba[1,2,5], Shin Nabatame[3,5], Yoshitaka Iijima[4], Kiyomi Nishiyama[1], Yoshinori Tsurusaki[1], Mitsuko Nakashima[1], Noriko Miyake[1], Fumiaki Tanaka[2], Keiichi Ozono[3], Hirotomo Saitsu[1] and Naomichi Matsumoto[1]

Rett syndrome (RTT) is a neurodevelopmental disorder mostly caused by *MECP2* mutations. We identified a *de novo WDR45* mutation, which caused a subtype of neurodegeneration with brain iron accumulation, in a patient showing clinically typical RTT. The mutation (c.830 + 1G > A) led to aberrant splicing in lymphoblastoid cells. Sequential brain magnetic resonance imaging demonstrated that iron deposition in the globus pallidus and the substantia nigra was observed as early as at 11 years of age. Because the patient showed four of the main RTT diagnostic criteria, *WDR45* should be investigated in patients with RTT without *MECP2* mutations.
Journal of Human Genetics (2014) **59,** 292–295; doi:10.1038/jhg.2014.18; published online 13 March 2014

Keywords: β-propeller protein-associated neurodegeneration (BPAN); neurodegeneration with brain iron accumulation; Rett syndrome; static encephalopathy of childhood with neurodegeneration in adulthood; *WDR45*

INTRODUCTION

Rett syndrome (RTT) is a neurodevelopmental disorder characterized by regression, loss of acquired purposeful hand skill and language, gait abnormalities and stereotypic hand movements.[1] In typical RTT, *MECP2* mutations can be found in 95–97% of cases, and *CDKL5* and *FOXG1* mutations have been found in atypical RTT.[1] Recently, mutations in *WDR45*, which plays an important role in autophagy, have been identified in a novel subtype of neurodegeneration with brain iron accumulation, called β-propeller protein-associated neurodegeneration (BPAN), which is formerly designated as static encephalopathy of childhood with neurodegeneration in adulthood.[2–4] BPAN shows an unprogressive course during childhood, sudden-onset severe dystonia-parkinsonism and progressive dementia in adulthood. Characteristic brain magnetic resonance imaging findings include iron deposition in the globus pallidus and substantia nigra, and hyperintensity of the substantia nigra with a central band of hypointensity in T1-weighted images.[3] Interestingly, 7 of 23 patients with a *WDR45* mutation showed Rett-like features, suggesting a possible involvement of *WDR45* mutations in RTT.[5] Here we report a patient with typical RTT possessing a *de novo WDR45* mutation.

MATERIALS AND METHODS

A 14-year-old Japanese girl was born to non-consanguineous parents as a first child after an uneventful pregnancy. There was no familial history of neurological diseases. Although her initial development was normal as she controlled her head at 4 months of age, developmental milestones were gradually delayed and she learned to walk at 1 year and 7 months. During infancy, she played with toys and started to talk at ~12 months of age. Her walking developed repetitive atonic episodes and an electroencephalogram showed focal irregular polyspikes and waves, and hence she was diagnosed with epilepsy. She was administered antiepileptic agents and carbamazepine was found to be effective. She gradually lost hand function and verbal communications by 4 years of age, and developed stereotypic hand movements such as continuous rubbing and licking, and dystonia. Although she now walks alone with an ataxic gait, her hand skills have regressed and she cannot talk. She shows hyperventilation, abnormally deep breathing, bruxism during waking periods, hypotonia, peripheral vasomotor disturbance, kyphosis, small cold hands and feet, sudden inappropriate laughing, diminished response to pain and intense eye communication. Sleep disturbance and microcephaly were unobserved. Brain magnetic resonance imaging at 3 and 4 years of age showed no remarkable findings (Figures 1a–d). However, T2-weighted images (WI) revealed mild hypointensity in the globus pallidus and the substantia nigra at 11 years of age (Figures 1e and f). At 14 years, this T2 shortening progressed (Figures 1g and h), and this hypointensity was obvious in T2*WI (Figures 2c

[1]Department of Human Genetics, Graduate School of Medicine, Yokohama City University, Yokohama, Japan; [2]Department of Clinical Neurology and Stroke Medicine, Yokohama City University, Yokohama, Japan; [3]Department of Pediatrics, Osaka University Graduate School of Medicine, Osaka, Japan and [4]Division of Pediatrics, Osaka Developmental Rehabilitation Center, Osaka, Japan
Correspondence: Professor N Matsumoto and Dr H Saitsu, Department of Human Genetics, Yokohama City University Graduate School of Medicine, 3-9 Fukuura, Kanazawa-ku, Yokohama 236-0004, Japan.
E-mail: naomat@yokohama-cu.ac.jp or hsaitsu@yokohama-cu.ac.jp
[5]These authors contributed equally as first authors.
Received 13 January 2014; revised 10 February 2014; accepted 18 February 2014; published online 13 March 2014

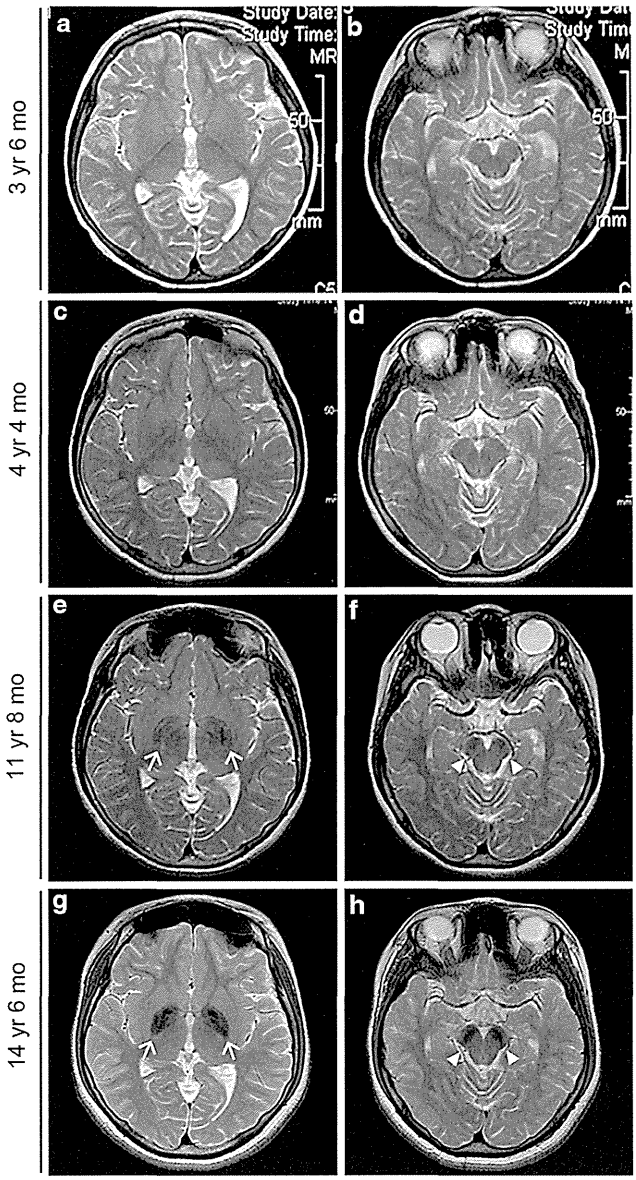

Figure 1 T2-weighted axial images of the patient with a *WDR45* mutation. (**a–h**) T2-weighted axial images of the patient. ((**a**, **b**) at 3 years and 6 months; (**c**, **d**) at 4 years and 4 months; (**e**, **f**) at 11 years and 8 months; (**g**, **h**) at 14 years and 6 months) Brain magnetic resonance imaging (MRI) at 3 and 4 years revealed no remarkable findings in the brain structure, volume and signal intensity (**a–d**). Mild T2 hypointensity in the globus pallidus (**e**, arrow) and the substantia nigra (**f**, arrowhead) was noticed at 11 years of age. At 14 years, T2WI showed strong hypointensity in the globus pallidus (**g**, arrow) and the substantia nigra (**h**, arrowhead). mo, months; yr, years.

and d). T1WI showed hyperintensity of the substantia nigra with a weak central band of T1WI hypointensity (Figure 2b). Experimental protocols for genetic analysis were approved by the Institutional Review Board of Yokohama City University School of Medicine. Clinical information and peripheral blood samples were acquired from family members after obtaining written informed consent.

Sanger sequencing

MECP2 mutation was sequenced by Sanger method. Parental samples were also sequenced with respect to identified variants.

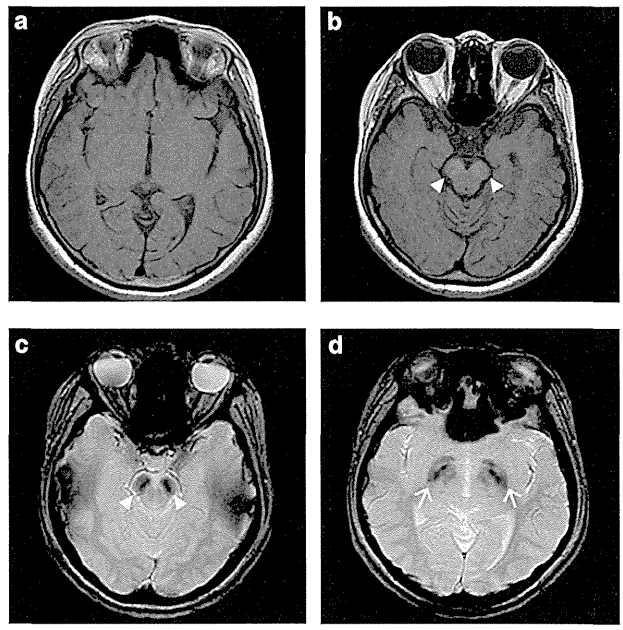

Figure 2 Brain magnetic resonance imaging (MRI) of the patient at 14 years of age. T1-weighted (**a**, **b**), and T2*-weighted (**c**, **d**) axial images of the patient at 14 years and 6 months of age. T1-weighted images show normal findings in the globus pallidus (**a**), but hyperintensity of the substantia nigra with a weak central band of T1WI hypointensity (**b**, arrowhead). T2*-weighted images show strong hypointensity in the substantia nigra (**c**, arrowhead) and the globus pallidus (**d**, arrow).

Whole exome sequencing

Genomic DNA was isolated from peripheral blood leukocytes using QuickGene 610L (Wako, Osaka, Japan), captured using the SureSelect Human All Exon v4 Kit (51 Mb; Agilent Technologies, Santa Clara, CA, USA) and sequenced on an Illumina HiSeq2000 (Illumina, San Diego, CA, USA) with 101 bp paired-end reads. Four samples were run in one lane of the flow cell. Exome data processing, variant calling and variant annotation were performed as previously described.[4] The *WDR45* mutation was confirmed by Sanger sequencing.

Reverse transcriptase-PCR

Lymphoblastoid cell lines were established from the patient. Reverse transcriptase-PCR using total RNA extracted from lymphoblastoid cell lines was performed as previously described.[6] Briefly, total RNA was extracted using the RNeasy Plus Mini kit (Qiagen, Tokyo, Japan), and 4 μg subjected to reverse transcription. For PCR, 2 μl of complementary DNA was used with primer ex8-9-F spanning exons 8 and 9 (5′-GTGGACCTGGCGAGCACAAAG-3′) and primer ex11-12-R spanning exons 11 and 12 (5′-AACTCTGTCATT GCCATCTGCGTAG-3′). The PCR reaction consisted of five cycles of 98 °C for 10 s, 72 °C for 30 s, five cycles of 98 °C for 10 s, 70 °C for 30 s, five cycles of 98 °C for 10 s, 68 °C for 30 s and 30 cycles of 98 °C for 10 s, 66 °C for 30 s. PCR products were electrophoresed on a 10% polyacrylamide gel and sequenced. PCR products were purified using the QIAEXII Gel extraction kit (Qiagen).

RESULTS AND DISCUSSION

We detected c.602C>T (p.Sla201Val) mutation of *MECP2* in the patient by Sanger sequencing. However, we consider this mutation was not pathogenic because the mutation was inherited from her healthy mother. The mutation was also found in 3 males and 8 females of our 574 in-house control exomes (281 males and 293 females). By whole exome sequencing, we

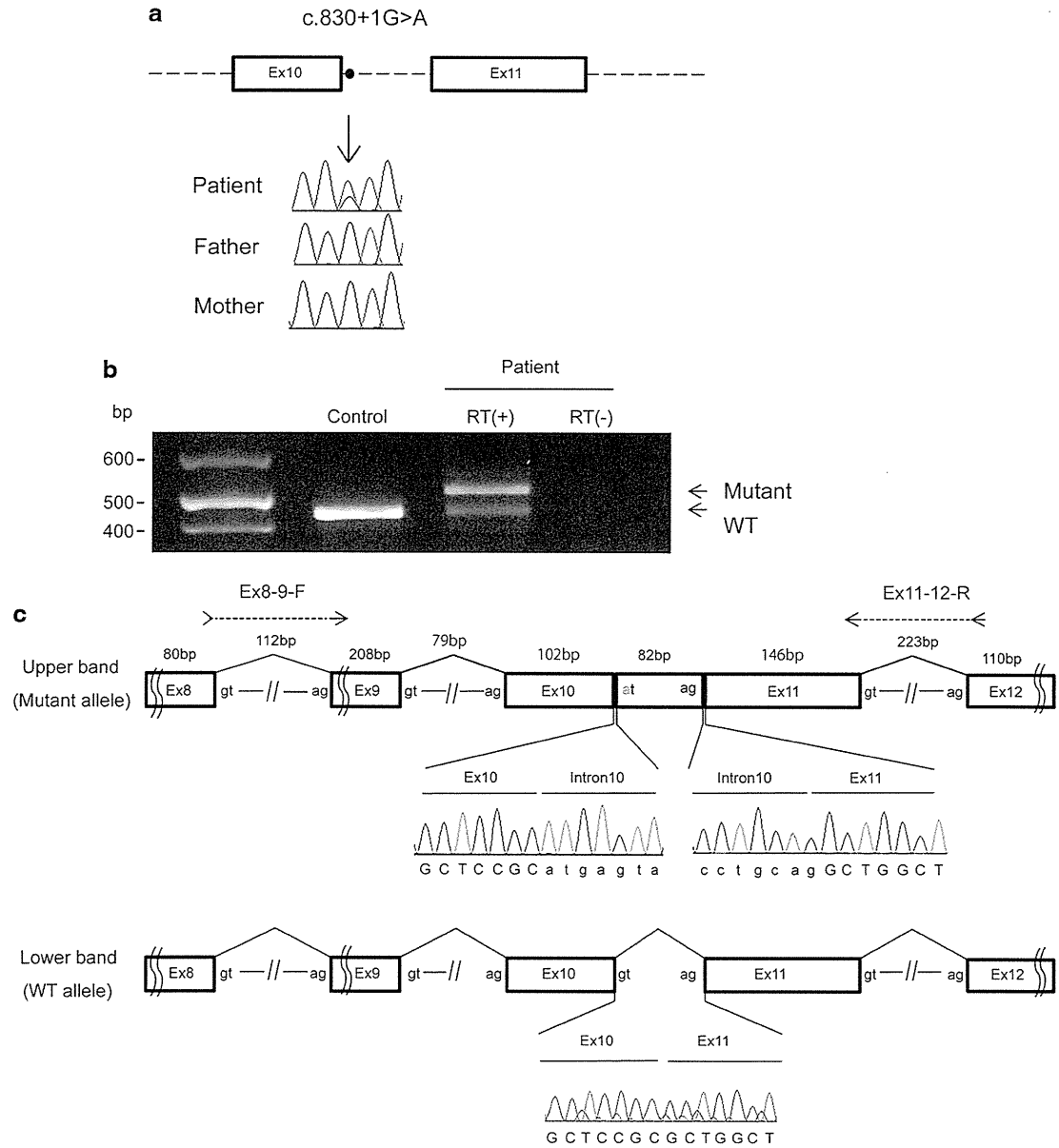

Figure 3 Mutation leading to aberrant splicing in the patient's lymphoblastoid cell lines. (**a**) Location of the *WDR45* mutation. A splice donor site mutation (c.830 + 1G > A) in the patient, which was absent from her parents, was confirmed by Sanger sequencing. (**b**) Reverse transcriptase (RT)-PCR analysis using lymphoblastoid cell lines derived from the patient and a control. A single band (472 bp), corresponding to the wild-type allele, was amplified using a control complementary DNA (cDNA) template. A longer aberrant band was detected from the patient's cDNA. (**c**) Schematic representation of the wild-type and mutant transcripts determined by sequencing PCR products, and primers used for the analysis. The upper band (551 bp) has a 82-bp insertion of the entire intron 10 sequence, leading to a frameshift. A full color version of this figure is available at the *Journal of Human Genetics* journal online.

identified a splice donor site mutation (c.830 + 1G > A) in the *WDR45* gene, which is absent from the proband's parents, indicating that the mutation occurred *de novo* (Figure 3a). The mutation was absent in the 6500 exomes sequenced by the National Heart, Lung, and Blood Institute exome project and our 574 in-house control exomes. Reverse transcriptase-PCR and sequencing revealed aberrant splicing in which 82 bp intronic sequences were retained by the use of a cryptic splice donor site within intron 10, generating a premature stop codon (p.Leu278*) (Figures 3b and c).

Although the brain magnetic resonance imaging at 11 years of age showed iron deposition in the globus pallidus and the substantia nigra, clinical features showed no aggravation at this time. Thus, there is no correlation between iron deposition and clinical phenotype. The fact that iron deposition preceded neurological decline is important information for elucidating BPAN pathogenesis that is caused by autophagy impairment.

The patient showed regression and stabilization, and fulfilled four of the main revised RTT diagnostic criteria,[1] indicating that she clinically showed typical RTT. In autopsied RTT brains, tyrosine hydroxylase activity is reduced in the substantia nigra, and may cause hypofunction of the nigrostriatal dopamine neurons involved in modulating posture and locomotion.[7] Dystonia and parkinsonism are also seen in older RTT patients as well as BPAN.[8]

Therefore, substantia nigra dysfunction might be involved in both RTT and BPAN, facilitating our understanding of the pathomechanism of RTT caused by *MECP2* mutations. We recommend that *WDR45* should be checked in RTT patients without *MECP2* mutation.

ACKNOWLEDGEMENTS

We thank the patient's family for their participation in this study. We also thank Nobuko Watanabe for her technical assistance. This work was supported by the Ministry of Health, Labour, and Welfare of Japan; the Japan Society for the Promotion of Science (a Grant-in-Aid for Scientific Research (B) from (25293085, 25293235), a Grant-in-Aid for Scientific Research (A) (13313587)); the Takeda Science Foundation; the fund for Creation of Innovation Centers for Advanced Interdisciplinary Research Areas Program in the Project for Developing Innovation Systems; the Strategic Research Program for Brain Sciences (11105137); and a Grant-in-Aid for Scientific Research on Innovative Areas (Transcription Cycle) from the Ministry of Education, Culture, Sports, Science and Technology of Japan (12024421).

1 Neul, J. L., Kaufmann, W. E., Glaze, D. G., Christodoulou, J., Clarke, A. J., Bahi-Buisson, N. *et al.* Rett syndrome: revised diagnostic criteria and nomenclature. *Ann. Neurol.* **68,** 944–950 (2010).
2 Haack, T. B., Hogarth, P., Kruer, M. C., Gregory, A., Wieland, T., Schwarzmayr, T. *et al.* Exome sequencing reveals de novo *WDR45* mutations causing a phenotypically distinct, X-linked dominant form of NBIA. *Am. J. Hum. Genet.* **91,** 1144–1149 (2012).
3 Kruer, M. C., Boddaert, N., Schneider, S. A., Houlden, H., Bhatia, K. P., Gregory, A. *et al.* Neuroimaging features of neurodegeneration with brain iron accumulation. *AJNR Am. J. Neuroradiol.* **33,** 407–414 (2012).
4 Saitsu, H., Nishimura, T., Muramatsu, K., Kodera, H., Kumada, S., Sugai, K. *et al. De novo* mutations in the autophagy gene *WDR45* cause static encephalopathy of childhood with neurodegeneration in adulthood. *Nat. Genet.* **45,** 445–449, 449e441 (2013).
5 Hayflick, S. J., Kruer, M. C., Gregory, A., Haack, T. B., Kurian, M. A., Houlden, H. H. *et al.* beta-Propeller protein-associated neurodegeneration: a new X-linked dominant disorder with brain iron accumulation. *Brain* **136,** 1708–1717 (2013).
6 Saitsu, H., Kato, M., Mizuguchi, T., Hamada, K., Osaka, H., Tohyama, J. *et al. De novo* mutations in the gene encoding STXBP1 (MUNC18-1) cause early infantile epileptic encephalopathy. *Nat. Genet.* **40,** 782–788 (2008).
7 Segawa, M. Early motor disturbances in Rett syndrome and its pathophysiological importance. *Brain. Dev.* **27** (Suppl 1), S54–S58 (2005).
8 FitzGerald, P. M., Jankovic, J., Glaze, D. G., Schultz, R. & Percy, A. K. Extrapyramidal involvement in Rett's syndrome. *Neurology* **40,** 293–295 (1990).

小児の難治性てんかんとCDKL5

田中輝幸　奥田耕助

はじめに

近年，乳児難治性てんかんの原因遺伝子として，*cyclin-dependent kinase-like 5*(*CDKL5*)が同定された．*CDKL5*はMAPキナーゼと相同性を持つセリン・スレオニンキナーゼCDKL5をコードする．*CDKL5*変異に伴う病態は，生後5ヵ月未満より発症する難治性てんかん，言語発達の欠失と，手の常同運動・頭囲発達障害などのRett症候群様症状を伴う重度の精神遅滞という特徴的な病像から，一疾患単位として認識されつつある．本稿では*CDKL5*に焦点を当て，ゲノム構造，遺伝子変異に伴う病像と変異解析，分子機能などを，既報告をもとに概説する．

*CDKL5*遺伝子とは

*CDKL5*遺伝子は，元々1998年，ヒトのXp22.3-p21.3領域の転写地図作製プロジェクトで*serine-threonine kinase 9*(*STK9*)としてクローニングされ，その後*cyclin-dependent kinase*(*CDK*)ファミリーとの相同性から，HUGO Gene Nomenclature Committee(HGNC)においてあらためて*cyclin-dependent kinase-like*(*CDKL*)遺伝子ファミリーの一員として*CDKL5*と命名された[1]．CDKLファミリーはCDKL1～CDKL5の5つのセリン・スレオニンキナーゼからなるが，キナーゼドメインがCDK，MAPキナーゼファミリーと高い配列類似性を持ち，518種類に及ぶヒトの全キナーゼの中でCMGC(CDK，MAPK，GSK3，CLK)グループに属する[2]．

ヒトの*CDKL5*遺伝子はXp22の228 kbにわたり，24のエクソン(1，1a，1b，2-16，16b，17-21)からなる．翻訳開始点はエクソン2に存在し，選択的スプライシングにより，イントロン18で終止する遺伝子産物(mRNA：3136 bp，蛋白：960アミノ酸，107 kDa)と，エクソン21で終止する遺伝子産物(mRNA：3434 bp，蛋白：1030アミノ酸，115 kDa)が生じる(図1)[3]．前者(107 kDa型)は脳に最も強く，ほぼ全身の組織に発現するが，後者(115 kDa型)は精巣特異的に発現する[4]．更に，選択的スプライシングによりエクソン16-17間にエクソン16b(123 bp，41アミノ酸分)が挿入された転写産物が，ほぼ脳特異的に発現する[5]．

CDKL5蛋白は，CDK，MAPキナーゼと相同性のキナーゼドメインをN末端側(エクソン2-11)に持ち，MAPキナーゼと同様にドメイン内のTEY(Thr-Glu-Tyr)モチーフを自己リン酸化する(図2)[6]．MAPキナーゼやCDKにない特徴として，CDKL5はC末端側に700アミノ酸にわたる長い配列をもつ．CDKL5はニューロン内で核と細胞質の両区画に局在し，NIH3T3細胞，HEK293細胞への強制発現実験によって，キナーゼ活性とC末端側領域が細胞質-核の局在を調節することが示されている[7,8]．

*CDKL5*は当初疾患との関連は不明であったが，2003年にその変異がX連鎖性点頭てんかん患児で同定されて以来，難治性てんかんの原因遺伝子として注目されることになった[9]．

*CDKL5*遺伝子変異

1．臨床的特徴

これまで文献では約100例の*CDKL5*遺伝子変異症例が報告されている．多くに共通する特徴は，① 妊娠期は正常，② けいれん発症前の周産期における過敏性，傾眠傾向，哺乳不良，③ 5ヵ月未満発症の難治性乳児けいれん，④ 頭囲発達の不良・常同行動・自発的な手の動きの欠失・睡眠障害等のRett症候群様の症状，⑤ 言語の欠失と視線が合わない異常を伴う重度の精神遅滞，であり，**早期発症の難治性てんかんと，Rett症候群様症状**がその中核である．けいれん発作としては点頭てんかん，ミオクロニーけいれんが最も頻度が高いが，経過を通じて複雑部分発作，全般性強直間代発作，強直発作等，多種に及ぶ[10]．病像は成長と

たなか てるゆき　東京大学大学院准教授/医学系研究科発達医科学
おくだ こうすけ　東京大学大学院/医学系研究科発達医科学

0289-0585/13/¥500/論文/JCOPY

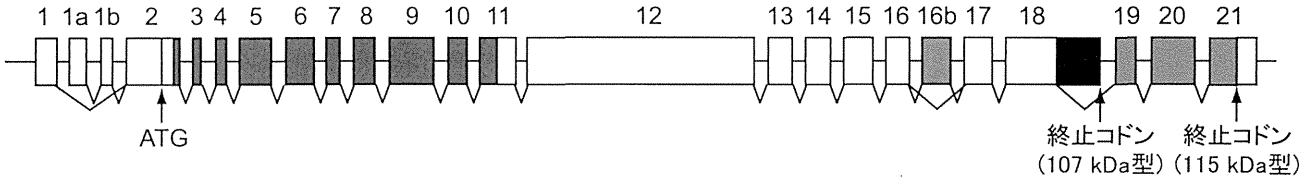

図 1 ヒト *CDKL5* 遺伝子のゲノム構造

ヒト *CDKL5* は 24 のエクソンからなる．翻訳開始点はエクソン 2 に存在し，選択的スプライシングにより，イントロン 18 で終止する遺伝子産物(107 kDa 型)，エクソン 21 で終止する遺伝子産物(115 kDa 型)，更にエクソン 16-17 間にエクソン 16b(123 bp)が挿入された遺伝子産物が生じる．薄紫色は非翻訳領域，青色はキナーゼドメイン，緑色，黒色，赤色はアイソフォーム特異的配列を示す．図中の各エクソン長は塩基数に応じてスケールを合わせた(イントロン長は任意)．(Kilstrup-Nielsen ら[3]より改変)

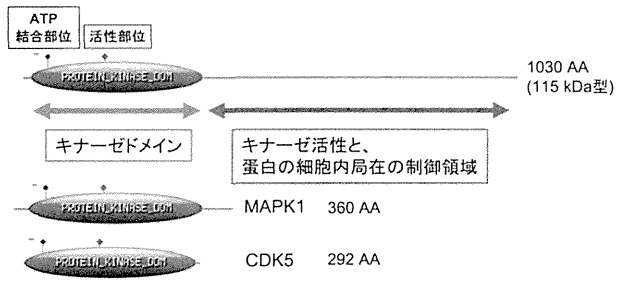

図 2 CDKL5 蛋白

CDKL5 蛋白は，AA 13-297 にキナーゼドメイン，AA 19-43 に ATP 結合部位，AA 131-143 に活性部位，AA 169-171 に TEY(Thr-Glu-Tyr)モチーフを有する．MAPK1，CDK5 と比較すると C 末端側の長い配列が際立つ特徴であり，この領域がキナーゼ活性および蛋白の細胞内局在を制御する．

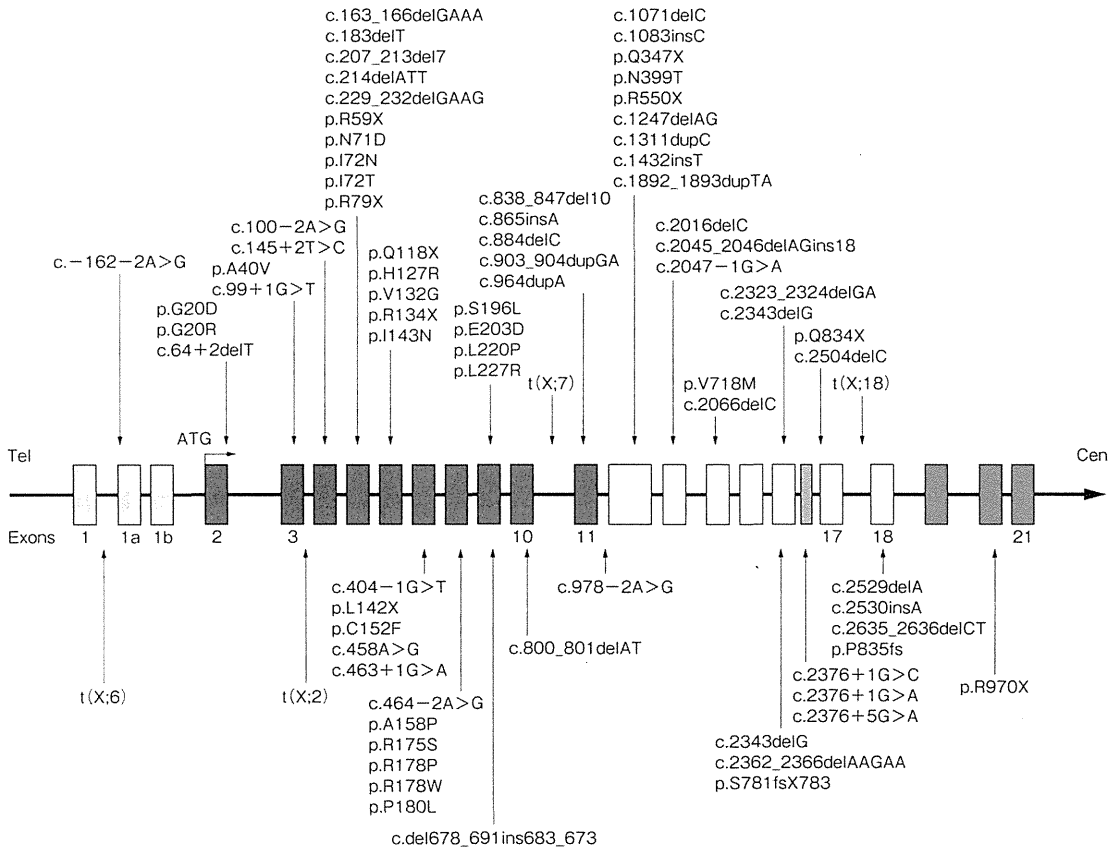

図 3 *CDKL5* 遺伝子変異

これまでに報告された変異部位を示す．1 例(p.V718M)を除き，全てのミスセンス変異はキナーゼドメインに対応するエクソン 2-11 内に限局するが，その他の変異は遺伝子全体にわたり分布する．(Bahi-Buisson ら[12]より)

共に変化し，年齢に応じて「早期乳児てんかん性脳症2型 early infantile epileptic encephalopathy-2(EIEE2)(OMIM #300672)」(乳児期早期)，「X連鎖性点頭てんかん・精神遅滞」(乳児期)，「非定型Rett症候群Hanefeld変異型」(幼児期以降)といった診断名が付けられている．Bahi-Buissonらは，*CDKL5*遺伝子変異を伴う2〜19歳までの13例の後方視的研究を行い，そのてんかんの経過を次の3つのステージに特徴付けた．

ステージ1： 生後1〜10週で発症する頻回のけいれん発作と，発作間欠期脳波は正常(9例)か基礎律動の軽度徐波化(4例)が特徴の「早期てんかん」期．発作型は顔面潮紅を伴う全般発作(10例)，全般間代発作(2例)で，持続は短く，しばしば1分以内であるが，高頻度(連日)に繰り返す．全例で粗大運動と筋緊張の低下と，視線が合わない異常が認められた．

ステージ2： 生後6ヵ月〜3歳の，点頭てんかん(8/8例)と脳波上ヒプスアリスミア(8/8例)を伴う「てんかん性脳症」期．著しい精神遅滞，筋緊張の低下，言語・視覚的コミュニケーションの消失，発達の停止が特徴である．

ステージ3： 生後2歳半以降の，「後期多焦点性・ミオクロニーてんかん」期．評価時に，6症例で前ステージの点頭てんかん(全例でステロイド治療に不応)から重度難治性てんかんに移行していた．発作型は強直発作・スパスム(4例)，ミオクローヌス(3例)，非定型欠神発作(2例)で，10回/日以上頻発し，抗けいれん薬，ケトン食とも全く無効，発作間欠期脳波は，高振幅棘波・多棘波の繰り返し群発を伴う高振幅徐波であった[11]．

2．遺伝子変異解析

*CDKL5*遺伝子変異はX連鎖優性遺伝であり，原則としてヘテロ接合体(2本のX染色体のうち1本に変異を持つ)の女性と，ヘミ接合体(唯一のX染色体に変異を持つ)の男性が発症する．既報告は1例を除き全てde novo(突然)変異であり，種々の点変異，欠失，更に重複が同定されている．

点変異としてはこれまで，23のミスセンス変異，10のナンセンス変異，25のフレームシフト変異，14のスプライス異常が報告されている[12]．重要な特徴として，1例を除く全てのミスセンス変異は，N末端側のキナーゼドメインに対応するエクソン2-11内に限局するが，それ以外の点変異は遺伝子全体にわたり分布する(図3)．組換え蛋白を用いた研究によって，キナーゼドメイン内のミスセンス変異はCDKL5キナーゼ活性を低下させることが示されている[6]．ミスセンス以外の点変異は結果的に中途終止コドン(premature termination codon, PTC)を生じるが，転写後，PTCを持つ異常mRNAの多くはナンセンス変異依存mRNA分解機構(nonsense-mediated mRNA decay, NMD)によって分解を受け，NMDが機能するルールに外れたmRNAのみ分解を免れる．つまり，*CDKL5*の点変異は，①(ミスセンスの場合)キナーゼ活性の低下，②(NMDを受けた場合)蛋白自体の消失，あるいは，③(NMDを免れた場合)C末端側が短縮した蛋白生成のいずれかを招く．①と②の場合は，キナーゼ活性の低下または消失を来すため，その病態は機能喪失(loss-of-function)といえるが，③の場合，変異蛋白がどのような作用を持つかによってその病態機序は異なることになる．これまでの研究で，C末端側を切断した組換えCDKL5変異体はキナーゼ活性が亢進すること，培養細胞への強制発現実験でより強く核へ集積することなどが示されており，病態機序として機能喪失以外のメカニズムも示唆されるが，実際の患者において短縮型mRNAおよび蛋白が安定して発現しているかどうかは確認されていない[6,8]．

点変異以外に，遺伝子の全長あるいは一部を含む欠失も複数報告されている[13]．また興味深いことに*CDKL5*遺伝子の重複例も報告されており，遺伝子量の増加も疾患を起因することが示唆される[14,15]．今後*CDKL5*遺伝子変異解析では，塩基配列のみならずアレイCGHあるいはmultiplex ligation-dependent probe amplification assay(MLPA)を用いたゲノム領域欠失，重複も視野に入れた探索を行うことが望ましい．

*CDKL5*変異に伴う病像には症状と重症度ともに幅があるが，今のところ明らかな遺伝子型-表現型連関(genotype-phenotype correlation)は確立されていない．

*CDKL5*は古典的Rett症候群の原因遺伝子*MECP2*(*methyl CpG binding protein 2*)と同じくX連鎖遺伝子であることから，当初スクリーニングの母集団が女児中心であり，変異報告例も女児がほとんどであった．しかし近年，男児における遺伝子変異の報告が相次ぎ，男児例は決して稀でない[16,17]．男児例はより重症度が高いという報告と，

性差はないとする報告とあるが，その差はスクリーニング母集団の偏りなどに起因すると考えられる．また，既報告では約1割が男児であるが，正確な男女比は未だ不明である．今後，*CDKL5*の遺伝子変異検査は性別に関わりなく行われる必要がある．

CDKL5分子機能

現在，われわれを含む多くの研究室でCDKL5の機能と遺伝子変異による病態機序解明のための研究が行われている．知見は未だ断片的であり全容解明には程遠いが，既報告からいくつかを概説する．

CDKL5は前述のように核と細胞質に局在することから，複数の異なる分子機能を持つと考えられる．核内作用に関して，これまでCDKL5のリン酸化基質としてMECP2およびDNA methyltransferase 1(DNMT1)が同定され，これらを介したエピジェネティック制御に関与する可能性がある[18,19]．また，CDKL5は核内でスプライシング因子の集積した“nuclear speckles”と呼ばれる構造に局在し，キナーゼ活性がその形成・動態を負に制御することから，CDKL5が遺伝子のRNAプロセシング，スプライシングに関与する可能性も考えられる[20]．一方，細胞質内においてCDKL5は，アクチンリモデリングに重要な役割を担うRho-GTPase Rac1と相互作用し，BDNF(brain-derived neurotrophic factor)-Rac1シグナリングを介して神経細胞樹状突起の形態形成を制御する[21]．更にCDKL5は，興奮性ニューロンのシナプス後肥厚部においてNGL-1をリン酸化し，NGL-1とPSD95の相互作用調節を介してシナプス安定性を制御する[22]．

むすび

*CDKL5*遺伝子変異は，特徴的な病像より，早期に遺伝子診断可能な難治性てんかん症候群である．その症状の永続性と重篤性から患者と家族の苦しみと負担は長く大きく，その解決は現代医学における最重要課題の一つである．今後，病態機序の解明と効果的治療法の開発のため，より多くの分子遺伝学的データの蓄積と分子機能研究の推進が必要不可欠である．

文献

1) Montini E, Andolfi G, Caruso A, et al. Identification and characterization of a novel serine-threonine kinase gene from the Xp22 region. Genomics. 1998；51：427-33.
2) Manning G, Whyte DB, Martinez R, et al. The protein kinase complement of the human genome. Science. 2002；298：1912-34.
3) Kilstrup-Nielsen C, Rusconi L, La Montanara P, et al. What we know and would like to know about CDKL5 and its involvement in epileptic encephalopathy. Neural Plast. 2012；2012：728267.
4) Williamson SL, Giudici L, Kilstrup-Nielsen C, et al. A novel transcript of cyclin-dependent kinase-like 5(CDKL5)has an alternative C-terminus and is the predominant transcript in brain. Hum Genet. 2012；131：187-200.
5) Fichou Y, Nectoux J, Bahi-Buisson N, et al. An isoform of the severe encephalopathy-related CDKL5 gene, including a novel exon with extremely high sequence conservation, is specifically expressed in brain. J Hum Genet. 2011；56：52-7.
6) Bertani I, Rusconi L, Bolognese F, et al. Functional consequences of mutations in CDKL5, an X-linked gene involved in infantile spasms and mental retardation. J Biol Chem. 2006；281：32048-56.
7) Lin C, Franco B, Rosner MR. CDKL5/Stk9 kinase inactivation is associated with neuronal developmental disorders. Hum Mol Genet. 2005；14：3775-86.
8) Rusconi L, Salvatoni L, Giudici L, et al. CDKL5 expression is modulated during neuronal development and its subcellular distribution is tightly regulated by the C-terminal tail. J Biol Chem. 2008；283：30101-11.
9) Kalscheuer VM, Tao J, Donnelly A, et al. Disruption of the serine/threonine kinase 9 gene causes severe X-linked infantile spasms and mental retardation. Am J Hum Genet. 2003；72：1401-11.
10) Bahi-Buisson N, Nectoux J, Rosas-Vargas H, et al. Key clinical features to identify girls with CDKL5 mutations. Brain. 2008；131：2647-61.
11) Bahi-Buisson N, Kaminska A, Boddaert N, et al. The three stages of epilepsy in patients with CDKL5 mutations. Epilepsia. 2008；49：1027-37.
12) Bahi-Buisson N, Bienvenu T. CDKL5-related disorders：from clinical description to molecular genetics. Mol Syndromol. 2012；2：137-52.
13) Van Esch H, Jansen A, Bauters M, et al. Encephalopathy and bilateral cataract in a boy with an interstitial deletion of Xp22 comprising the CDKL5 and NHS genes. Am J Med Genet A. 2007；143：364-9.
14) Tzschach A, Chen W, Erdogan F, et al. Characterization of interstitial Xp duplications in two families by tiling path array CGH. Am J Med Genet A. 2008；146A：197-203.
15) Froyen G, Van Esch H, Bauters M, et al. Detection of genomic copy number changes in patients with idiopathic mental retardation by high-resolution X-array-CGH：important role for increased gene dosage of XLMR genes. Hum Mutat. 2007；28：1034-42.
16) Liang JS, Shimojima K, Takayama R, et al. CDKL5 alterations lead to early epileptic encephalopathy in both genders. Epilepsia. 2011；52：1835-42.
17) Elia M, Falco M, Ferri R, et al. CDKL5 mutations in boys with severe encephalopathy and early-onset intractable epilepsy. Neurology. 2008；71：997-9.
18) Kameshita I, Sekiguchi M, Hamasaki D, et al. Cyclin-dependent kinase-like 5 binds and phosphorylates DNA methyltransferase 1. Biochem Biophys Res Commun. 2008；377：1162-7.
19) Mari F, Azimonti S, Bertani I, et al. CDKL5 belongs to the same molecular pathway of MeCP2 and it is responsible for the early-onset seizure variant of Rett syndrome. Hum Mol Genet. 2005；14：1935-46.
20) Ricciardi S, Kilstrup-Nielsen C, Bienvenu T, et al. CDKL5 influences RNA splicing activity by its association to the nuclear speckle molecular machinery. Hum Mol Genet. 2009；18：4590-602.
21) Chen Q, Zhu YC, Yu J, et al. CDKL5, a protein associated with Rett syndrome, regulates neuronal morphogenesis via Rac1 signaling. J Neurosci. 2010；30：12777-86.
22) Ricciardi S, Ungaro F, Hambrock M, et al. CDKL5 ensures excitatory synapse stability by reinforcing NGL-1-PSD95 interaction in the postsynaptic compartment and is impaired in patient iPSC-derived neurons. Nat Cell Biol. 2012；14：911-23.